On The Dynamic Calibration and Trajectory Control of ARASH:ASiST

A. Hassani*, M.R. Dindarloo*, R. Khorrambakht*, A. Bataleblu*, R. Heidari*,
M. Motaharifar†, S. F. Mohammadi‡, H. D. Taghirad*
* Advanced Robotics and Automated Systems (ARAS), K.N. Toosi University of Technology, Tehran, Iran.
† Department of Electrical Engineering, University of Isfahan, Isfahan, Iran.
‡ Translational Ophthalmology Research Center, Farabi Eye Hospital,
Tehran University of Medical Sciences, Tehran, Iran.
Email: * taghirad@kntu.ac.ir, † m.motaharifar@eng.ui.ac.ir, ‡ sfmohammadi@tums.ac.ir

***Abstract*—This article investigates the dynamic parameter calibration of ARAS Haptic System for EYE Surgery Training (ARASH:ASiST). ARASH:ASiST is a 3–DOF haptic device developed for intraocular surgery training. In this paper, the linear regression form of the dynamic formulation of the system with respect to its dynamic parameters is derived. Then the dynamic parameters of ARASH:ASiST are calibrated using the least square (LS) identification scheme. The cross–validation results for different trajectories indicate that the identified model has a suitable approximate fitness percentage in both translational and rotational motions of the surgical instrument. Finally, a robust model-based controller is implemented on the real prototype by the use of the calibration outcome, and it is verified that by using the estimated dynamic model, the trajectory tracking performance is significantly improved and the tracking error is reduced 50% compared to that of using the nominal dynamic model of the robot.**

***Index Terms*—ARASH:ASiST, Robot-Assisted Surgery, Dynamics Analysis, Dynamic Parameter Identification, Precisions.**

I. Introduction

One of the most challenging operations in clinical practice is intraocular eye surgery. Human eyes are delicate and highly complex organs, and the accuracy required for most intraocular surgeries ranges from $50 - 100\mu m$ [1]. Typically, intraocular surgeries are considered as a micro-surgical procedure, and during surgery, surgeons must carefully control the position and force of a small surgical instrument in an area of limited workspace with a delicate positioning accuracy. In order to address these challenges, robotic technology may come to the rescue. By using robot–assisted surgery, surgeons can perform microsurgeries with high levels of accuracy and dexterity, in a comfortable and ergonomic environment. In recent years, various surgical eye robots for intraocular surgeries have been developed, some of them have been reported in [2]. Moreover, the process of training novice eye surgeons can also be evaluated using micro-surgical robots [3].

In this context, ARASH:ASiST has been developed in *Advanced Robotics and Automated Systems (ARAS)* for eye surgery training. This device has 3-DOF haptic interface, developed for use in a dual haptic eye surgery training system [4]. Considering its mechanical features, this device provides the main required minimally invasive vitrectomy surgery properties, such as the remote center of motion and favorable kinematic workspace. ARASH:ASiST provides more than 90° in both rotational motions, $43.6mm$ in the insertion direction of the surgical instrument. Furthermore, it is equipped with two symmetrical weight counterbalances for weight compensation of the mechanism. A picture of the ARASH:ASiST system is shown in Figure 1.

It is essential to derive complete and accurate dynamic models of the surgical robots, for the use of model-based controller design in motion/force control, development of realistic simulators, collision detection, and force estimation of surgeon's hands [5]. As the first solution, computer-aided design (CAD) model of the robot may be used to extract inertial parameters properties of the manipulator. Due to the uncertainty of complex geometric bodies, and material densities, CAD models may not be accurate enough to estimate the true dynamics [6]. On the other hand, there are always structural uncertainties in practice, such as unmodeled dynamics, which reduce the accuracy of the model. One of the common ways to address this issue is to identify robot dynamics by the use of linear regression schemes. For this purpose, first, the linear regression form of the robot dynamics with respect

Fig. 1. ARASH:ASiST prototype

978-1-6654-9569-1/22/$31.00

to the robot dynamic parameters is derived. Since several regressor matrix elements are zero or linearly dependent on the others, the regressor matrix is usually not full rank, which causes some dynamic parameters to become unidentifiable. Therefore, a reduced regressor matrix is usually derived in which the base inertial parameters (BIP) are identified as the minimum number of independent inertial parameters to uniquely describe the robot dynamics [7].

Among the notable researches on the dynamic parameter identification of different surgical robots, references [5], [8] may be noticed. In these references, it is indicated that in case of persisting excitation trajectories, suitable data acquisition, signal processing, and using the least-squares method, a suitable estimate of the robot's dynamic BIP may be achievable. Considering this fact, this paper examines dynamic parameter calibration of ARASH:ASiST, which is of utmost importance for its further clinical practices. For this means, the linear regression form of robot dynamic with respect to dynamic parameters is derived, and then all the terms affecting robot dynamics are extracted. Then, the dynamic parameters of the robot are identified using LS technique, and the quality of identified model is examined by two different means. Finally, the precise motion tracking of ARASH:ASiST is experimented using a robust model-based controller, which uses identified dynamic model.

II. Dynamic Formulation

The overview of the ARASH:ASiST mechanism is shown in Figure 2. In dynamic analysis of this paper, $\boldsymbol{q} = [\phi, \psi, d]^T$ represents the actuated joints variables, while $\boldsymbol{\tau}$ is the generalized actuators forces $\boldsymbol{\tau} = [\tau_\phi, \tau_\psi, f_d]^T$. Moreover, by choosing spherical coordinate system, $\boldsymbol{q} = \boldsymbol{x} = [\phi, \psi, d]^T$ is considered as a way to the robot task–space variables [9].

A. Dynamic Analysis of Links

Dynamics formulations of manipulators may be expressed in linear form with respect to inertial parameters as [10]:

$$\boldsymbol{\tau}_{Links} = \boldsymbol{Y}_{Links}(\boldsymbol{q}, \dot{\boldsymbol{q}}, \ddot{\boldsymbol{q}})\boldsymbol{\pi}_{Links} \ , \ \in \mathbb{R}^3, \tag{1}$$

in which, $\boldsymbol{Y}_{Links}$ and $\boldsymbol{\pi}_{Links}$ denote the linear regressor and inertial parameters vector of the manipulator, respectively. To extract linear regressor form, the method developed in [11] is borrowed. By this means, the regressor matrix of ARASH:ASiST links may be derived as:

$$\boldsymbol{Y}_{Links} = \begin{bmatrix} \boldsymbol{Y}_i & \dots & \boldsymbol{Y}_n \end{bmatrix} \ , \ \in \mathbb{R}^{3\times 80}, \tag{2a}$$

$$\boldsymbol{Y}_i = \begin{bmatrix} \boldsymbol{Y}_{m_i} & \boldsymbol{Y}_{\rho_i} & \boldsymbol{Y}_{I_i} \end{bmatrix}. \tag{2b}$$

where, the components of $\boldsymbol{Y}_i$ are defined as:

$$\boldsymbol{Y}_{m_i} := \boldsymbol{J}_{v_{J_i}}{}^T \left({}^0\boldsymbol{a}_{J_i} - \boldsymbol{g}_0\right), \tag{3}$$

$$\begin{aligned} \boldsymbol{Y}_{\rho_i} := &+ \boldsymbol{J}_{v_{J_i}}{}^T \left({}^0\dot{\boldsymbol{\omega}}_{i_\times} + {}^0\boldsymbol{\omega}_{i_\times} {}^0\boldsymbol{\omega}_{i_\times} \right) {}^0\boldsymbol{R}_i \\ &- \boldsymbol{J}_{\omega_i}{}^T \left({}^0\boldsymbol{a}_{J_i} - \boldsymbol{g}\right)_\times {}^0\boldsymbol{R}_i, \end{aligned} \tag{4}$$

$$\boldsymbol{Y}_{I_i} := \boldsymbol{J}_{\omega_i}{}^T \left({}^0\boldsymbol{R}_i \, {}^i\tilde{\dot{\boldsymbol{\omega}}}_i + {}^0\boldsymbol{\omega}_{i_\times} {}^0\boldsymbol{R}_i \, {}^i\tilde{\boldsymbol{\omega}}_i \right). \tag{5}$$

In this representation, $\boldsymbol{J}_{v_{J_i}}$, and $\boldsymbol{J}_{\omega_i}$ denotes linear and angular Jacobian matrix of joint frame i, ${}^0\boldsymbol{a}_{J_i}$ is linear acceleration of joint frame i respect to base coordinate, ${}^0\boldsymbol{\omega}$ demonstrate angular velocity joint frame i respect to base coordinate, ${}^0\boldsymbol{R}_i$ is rotation matrix of joint frame i, and $\boldsymbol{g}$ is gravitational acceleration vector. Moreover, $\boldsymbol{x}_\times$ represent the 3×3 skew-symmetric matrix generated from the vector $\boldsymbol{x}$, and $\tilde{\boldsymbol{y}}$ of vector $\boldsymbol{y} = [y_1, y_2, y_3]^T$ may be defined as:

$$\tilde{\boldsymbol{y}} := \begin{bmatrix} y_1 & 0 & 0 & -y_2 & -y_3 & 0 \\ 0 & y_2 & 0 & -y_1 & 0 & -y_3 \\ 0 & 0 & y_3 & 0 & -y_1 & -y_2 \end{bmatrix}. \tag{6}$$

In previous study on ARASH:ASiST [4], the position vector ${}^0\boldsymbol{p}_{J_i}$, rotation matrix ${}^0\boldsymbol{R}_i$, and angular Jacobian matrix $\boldsymbol{J}_{\omega_i}$ of each coordinate frame system is reported in detail. To derive other components of equations (3) to (5), one may write $\boldsymbol{J}_{v_{J_i}} = \frac{\partial \, {}^0\boldsymbol{p}_{J_i}}{\partial \boldsymbol{q}}$, ${}^0\boldsymbol{a}_{J_i} = \boldsymbol{J}_{v_{J_i}}\ddot{\boldsymbol{q}} + \dot{\boldsymbol{J}}_{v_{J_i}}\dot{\boldsymbol{q}}$, and ${}^0\dot{\boldsymbol{\omega}}_i = \boldsymbol{J}_{\omega_i}\ddot{\boldsymbol{q}} + \dot{\boldsymbol{J}}_{\omega_i}\dot{\boldsymbol{q}}$. Moreover, the inertial parameters $\boldsymbol{\pi}$ are defined as:

$$\boldsymbol{\pi} = \begin{bmatrix} {\boldsymbol{\pi}_1}^T, ..., {\boldsymbol{\pi}_8}^T \end{bmatrix}^T \ , \ \in \mathbb{R}^{80}, \tag{7a}$$

$$\boldsymbol{\pi}_i = \begin{bmatrix} m_i, m_i \, {}^i\boldsymbol{\rho}_i^T, {}^i\bar{\boldsymbol{I}}_i{}^T \end{bmatrix}^T, \tag{7b}$$

in which, m_i, and ${}^i\boldsymbol{\rho}_i$ denote the mass, and the first moment vector of each link, respectively. Furthermore, ${}^i\bar{\boldsymbol{I}}_i$ denotes linear regression form of moment of inertia matrix of each link with respect to the joint frame i. This may be derived as ${}^i\bar{\boldsymbol{I}}_i = [I_{xx_i}, I_{yy_i}, I_{zz_i}, I_{xy_i}, I_{xz_i}, I_{yz_i}]^T$.

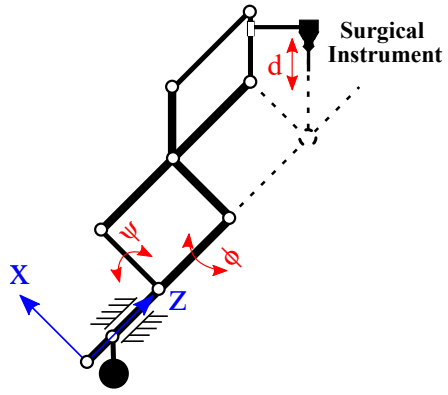

Fig. 2. Overview of kinematic structure of ARASH:ASiST

B. Friction Terms

For friction estimation of ARASH:ASiST, the common linear Coulomb plus viscous friction model is considered as $\boldsymbol{\tau}_f \approx \boldsymbol{F}_v\dot{\boldsymbol{q}} + \boldsymbol{F}_c sign(\dot{\boldsymbol{q}}) = \boldsymbol{Y}_f \ \boldsymbol{\pi}_f$. The most important reason for this choice is the linearity of the friction model and its comprehensiveness, despite the small parameters. The considered friction model may be written respect to friction terms as follows:

$$\boldsymbol{Y}_f = \begin{bmatrix} \dot{q}_1 & sgn(\dot{q}_1) & 0 & 0 & 0 & 0 \\ 0 & 0 & \dot{q}_2 & sgn(\dot{q}_2) & 0 & 0 \\ 0 & 0 & 0 & 0 & \dot{q}_3 & sgn(\dot{q}_3) \end{bmatrix}, \tag{8a}$$

$$\boldsymbol{\pi}_f = \begin{bmatrix} f_{v_1} & f_{c_1} & f_{v_2} & f_{c_2} & f_{v_3} & f_{c_3} \end{bmatrix}^T. \tag{8b}$$

C. Elastic Terms

By ignoring the terms of sagging, hysteresis, and viscoelastic terms of cables, the linear dynamics of ARASH:ASiST transmission cables may be estimated as $\boldsymbol{\tau}_e \approx \boldsymbol{K}_e\boldsymbol{q} = \boldsymbol{Y}_e\boldsymbol{\pi}_e$. Similarly, this model may be written with respect to elastic terms as follows:

$$\boldsymbol{Y}_e = diag\left(q_1, q_2, q_3\right), \quad \boldsymbol{\pi}_e = \begin{bmatrix} k_{e_1} & k_{e_2} & k_{e_3} \end{bmatrix}^T. \tag{9}$$

D. Full Regressor Formulation

Considering the dynamic terms affecting the robot dynamics, the overall generalized torques of ARASH:ASiST may be estimated as $\boldsymbol{\tau} \approx \boldsymbol{\tau}_{Links} + \boldsymbol{\tau}_f + \boldsymbol{\tau}_e = \boldsymbol{Y}(\boldsymbol{q}, \dot{\boldsymbol{q}}, \ddot{\boldsymbol{q}})\boldsymbol{\pi}$, in which full linear regressor $\boldsymbol{Y}$ and full dynamic parameters $\boldsymbol{\pi}$ may be derived as follow:

$$\boldsymbol{Y} = \begin{bmatrix} \boldsymbol{Y}_{Links} & \boldsymbol{Y}_f & \boldsymbol{Y}_e \end{bmatrix} \ , \ \in \mathbb{R}^{3\times 89}, \tag{10a}$$

$$\boldsymbol{\pi} = \begin{bmatrix} \boldsymbol{\pi}_{Links} & \boldsymbol{\pi}_f & \boldsymbol{\pi}_e \end{bmatrix} \ , \ \in \mathbb{R}^{89\times 1}. \tag{10b}$$

E. Regressor Reduction

In this section, unique solution of Ref. [12] is utilized to calculate BIP of ARASH:ASiST. The overdetermined linear model of robot dynamics may be formulated as:

$$\boldsymbol{\mathcal{T}} = \boldsymbol{W}(\boldsymbol{q}, \dot{\boldsymbol{q}}, \ddot{\boldsymbol{q}})\boldsymbol{\pi}, \tag{11}$$

in which, $\boldsymbol{W} = \begin{bmatrix} \boldsymbol{Y}(t_1)^T, ..., \boldsymbol{Y}(t_j)^T \end{bmatrix}^T$ represents the observation matrix, $\boldsymbol{\mathcal{T}} = \begin{bmatrix} \boldsymbol{\tau}(t_1)^T, ..., \boldsymbol{\tau}(t_j)^T \end{bmatrix}^T$ denotes the global torque vector, and j is the number of observations. Given the high number of observations, the reduced regressor matrix $\boldsymbol{Y}_r$ and base inertial parameters $\boldsymbol{\pi}_r$ would be extracted when the observation matrix $\boldsymbol{W}$ is full rank ($p = rank(\boldsymbol{W})$). The existence of a unique transformation matrix $\boldsymbol{B}$ with generalized inverse $\boldsymbol{B}^\dagger = \boldsymbol{S}\boldsymbol{B}^T\left(\boldsymbol{B}\boldsymbol{S}\boldsymbol{B}^T\right)^{-1}$ and matrix $\boldsymbol{S}$ may be proved, covering a base for the row space of the observation matrix [12].

In order to obtain the $\boldsymbol{B}$ matrix, it is necessary to determine the reduced–row echelon form of $\boldsymbol{W}$ to extract the upper triangular matrix of $\boldsymbol{B}_E$, which is a function of the kinematic parameters of the robot. Then, matrix $\boldsymbol{B}$ is obtained by eliminating the zero rows of $\boldsymbol{B}_E$. Therefore, $\boldsymbol{Y}_r$ and $\boldsymbol{\pi}_r$ of ARASH:ASiST may be elicited as:

$$\boldsymbol{Y}_r = \boldsymbol{Y}\boldsymbol{B}^\dagger \in \mathbb{R}^{3\times 23} \quad , \quad \boldsymbol{\pi}_r = \boldsymbol{B}\boldsymbol{\pi} \in \mathbb{R}^{23\times 1}. \tag{12}$$

Reduced-row echelon form[1] of $\boldsymbol{W}$ provides the unique BIP of the model.

III. Calibration

A. Least Squares Formulation

In this section, the LS-based dynamic parameter calibration of ARASH:ASiST is examined. By collecting sufficient m joint position sample measurements, as well as joint torque measurements, and the formation of stacking torque vector, and regressor matrix, the general identification problem may be written as:

$$\boldsymbol{\mathcal{T}} = \overline{\boldsymbol{Y}}_{\boldsymbol{r}}(\boldsymbol{q}, \dot{\boldsymbol{q}}, \ddot{\boldsymbol{q}})\boldsymbol{\pi}_r + \boldsymbol{\rho}, \tag{13}$$

in which, $\boldsymbol{\mathcal{T}} = \begin{bmatrix} \boldsymbol{\tau}(t_1) & ... & \boldsymbol{\tau}(t_m) \end{bmatrix}^T$ is the stacked vector of joint torque vectors, $\overline{\boldsymbol{Y}}_{\boldsymbol{r}}(\boldsymbol{q}, \dot{\boldsymbol{q}}, \ddot{\boldsymbol{q}}) = \begin{bmatrix} \boldsymbol{Y}_r(t_1) & ... & \boldsymbol{Y}_r(t_m) \end{bmatrix}^T$ denotes the stacked reduced regressor matrix, and $\boldsymbol{\rho}$ denotes the stacked measurement noise vector, which is assumed to be additive and zero mean Gaussian. Therefore, $\boldsymbol{\pi}_r$ may be estimated by solving the LS problem as:

$$\hat{\boldsymbol{\pi}}_r = \left(\overline{\boldsymbol{Y}}_{\boldsymbol{r}}{}^T\overline{\boldsymbol{Y}}_{\boldsymbol{r}}\right)\overline{\boldsymbol{Y}}_{\boldsymbol{r}}\boldsymbol{\mathcal{T}} = \overline{\boldsymbol{Y}}_{\boldsymbol{r}}{}^\dagger\boldsymbol{\mathcal{T}} \quad , \quad \in \mathbb{R}^{23\times 1}. \tag{14}$$

For the purpose of evaluating the accuracy of $\hat{\boldsymbol{\pi}}_r$ calibration, the relative standard deviation percentage of the individual parameter estimates is defined as a consistency measure [13], [14]:

$$\%\sigma_{\hat{\pi}_{r_i}} = 100\frac{\sigma_{\hat{\pi}_{r_i}}}{|\hat{\pi}_{r_i}|}, \tag{15}$$

in which, the covariance of the estimation error $\sigma_{\hat{\pi}_{r_i}}$ is calculated as:

$$\sigma_{\hat{\pi}_{r_i}} = \sqrt{diag\left(\sigma_p{}^2\left(\overline{\boldsymbol{Y}}_{\boldsymbol{r}}{}^T\overline{\boldsymbol{Y}}_{\boldsymbol{r}}\right)^{-1}\right)}, \tag{16}$$

and $\sigma_p{}^2$ is variance of the parameter estimation, and may be calculated as:

$$\sigma_p{}^2 = \frac{\|\boldsymbol{\mathcal{T}} - \overline{\boldsymbol{Y}}_{\boldsymbol{r}}(\boldsymbol{q}, \dot{\boldsymbol{q}}, \ddot{\boldsymbol{q}})\hat{\boldsymbol{\pi}}_r\|}{3m - 23}. \tag{17}$$

B. Persistently Exciting Trajectory

To design persistently exciting trajectory, which is rich enough in bandwidth while not exciting unmodeled dynamics terms, the composition of sinusoidal trajectories proposed in [15] is used. This may be represented by:

$$\boldsymbol{q}_i = \sum_{l=1}^{L} + \frac{{a_l}^i}{l\omega_f}\sin(l\omega_f\ t) - \frac{{b_l}^i}{l\omega_f}\cos(l\omega_f\ t) + \boldsymbol{q}_{i_0}, \tag{18}$$

in which, ω_f denotes the frequency of trajectory, and L demonstrates the number of the Fourier series harmonics. Moreover, the quantities ${a_l}^i$, ${b_l}^i$, and $\boldsymbol{q}_{i_0}$ for $l = 1, \cdots, L$ are the parameters, that should be optimized such that the generated trajectory is in the robot's feasible workspace and persistently excite the dynamics. Joint positions and velocity limits can be taken into account as:

$$\boldsymbol{q}_{min} < \boldsymbol{q}(T_s \cdot i) < \boldsymbol{q}_{max} \quad , \quad 0 < i < T_f/T_s, \tag{19a}$$

$$\dot{\boldsymbol{q}}_{min} < \dot{\boldsymbol{q}}(T_s \cdot i) < \dot{\boldsymbol{q}}_{max} \quad , \quad 0 < i < T_f/T_s. \tag{19b}$$

where $i = 0, 1, \cdots, T_f/T_s$, T_f is the final time, and T_s denotes the sampling time. The main time period of the trajectory $T = \frac{2\pi}{\omega_f}$ is set as $T = 15s$, and L have been set to $L = 5$, and $\boldsymbol{q}$ and $\dot{\boldsymbol{q}}$ limits are chosen as:

$$[-42.5, -25, -1.4]^T < \boldsymbol{q} < [+42.5, +55, +2.7]^T, \tag{20a}$$

$$[-200, -200, -100]^T < \dot{\boldsymbol{q}} < [+200, +200, +100]^T. \tag{20b}$$

[1] Use `rref` command in *MATLAB*.

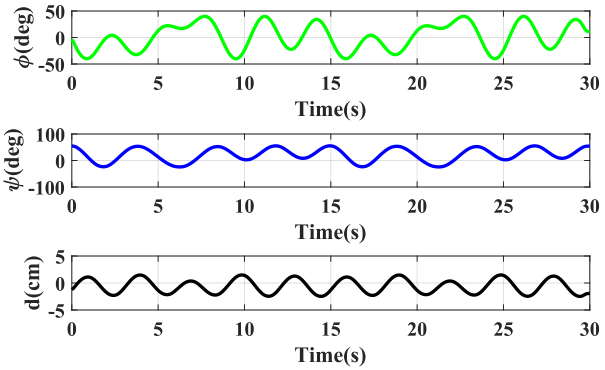

Fig. 3. Generated excitation trajectory in time domain

where, the dimensions of rotational motions in $\boldsymbol{q} = [\psi, \psi, d]$ is the degree and that of the linear motion is mm. The condition number of normalized $\boldsymbol{Y}_r$ is considered as objective function, and for solving this constrained nonlinear optimization problem, the *fmincon* command with *active-set* algorithm has been used [5]. The *cond* value has converged to 2.132 in the optimization process, and the generated trajectory can be seen in Figure 3.

C. Preprocessing of Experimental Data

For motion tracking control of the robot, inverse dynamic controller (IDC) with CAD data of robot dynamic parameters is experimented on the robot [4], and the designed excitation trajectory Figure 3 is tracked for $T_f = 300s$ with fixed sample time $T_s = 0.001$. Since the excitation trajectory is periodic, the logged data is divided into $T_f/T = 20$ separate sections. Therefore, for each sample time, there are 20 similar data sets, which are not exactly the same due to the effect of noise on the measurement[2]. Using the averaging technique, the effect of noise on $\boldsymbol{\tau}$ data, which is much noisier than $\boldsymbol{q}$ data, is desirably reduced. In order to calculate $\dot{\boldsymbol{q}}$, and $\ddot{\boldsymbol{q}}$, we filtered averaged $\boldsymbol{q}$ in an offline routine, using a noncausal zero-phase IIR Butterworth filter of order 5 both in forward and reverse direction[3]. Then, $\dot{\boldsymbol{q}}$, and $\ddot{\boldsymbol{q}}$ are estimated using a central difference algorithm to avoid lag and are filtered in the same way. Moreover, averaged joint torques are filtered in a similar manner with a low-pass IIR Butterworth filter.

IV. Validation

A. Evaluating Quality of Calibration

For the purpose of performance validation, the proposed trajectory is first examined in ARASH:ASiST by implementing nominal IDC controller. Then, relevant data are recorded using data acquisition system, and by reforming Eq. (13), reduced inertia parameters $\hat{\boldsymbol{\pi}}_r$, is identified using Eq. (14). For quantitative comparison of the torques resulting from identified parameters $\hat{\boldsymbol{\tau}}$, with measured torques of actuators $\boldsymbol{\tau}$, the following fitness percentage (FP) criteria, derived from the definition of normalized root mean square error (NRMSE), is used [16]:

$$FP\% = 100\left(1 - \frac{||\boldsymbol{\tau} - \hat{\boldsymbol{\tau}}||}{||\boldsymbol{\tau} - mean\,(\boldsymbol{\tau})\,||}\right), \qquad (21)$$

By taking the nominal CAD parameters of robot, and LS identification (14), the generalized torques $\boldsymbol{\tau}$ are denoted by $\hat{\boldsymbol{\tau}}_{CAD} = \boldsymbol{Y}_r(\boldsymbol{q}, \dot{\boldsymbol{q}}, \ddot{\boldsymbol{q}})\hat{\boldsymbol{\pi}}_{r_{(CAD)}}$, and $\hat{\boldsymbol{\tau}}_{LS} = \boldsymbol{Y}_r(\boldsymbol{q}, \dot{\boldsymbol{q}}, \ddot{\boldsymbol{q}})\hat{\boldsymbol{\pi}}_{r_{(LS)}}$, and their comparative studies is shown in. Figure 4. As shown in this figure, the CAD-based torque τ_ϕ has a relatively good approximation to the measured torques, but in ψ and d, the estimated torques from CAD data is poorly inaccurate. However, by using LS identification, more accurate estimates of generalized torques are obtained.

Moreover, to evaluate the quality of the calibration of each identified dynamic parameter, the consistency measure given in Eq. (15) is utilized, and the result is reported in Table I. By examining the results reported in this Table, it is seen that the consistency measure for all identified parameters is below 30%, which indicates that the LS identification process has been performed with good accuracy [14]. Furthermore, some base inertial parameters, have a physical meaning, such as π_{r_1} to π_{r_8}, and by comparing their identified values to the nominal values the accuracy and integrity of the calibration process in verified.

B. Cross Validation

In order to check the quality of the calibration in LS identification scheme, $\boldsymbol{q}$ is are considered as $\phi = 35° \sin(\omega t), \psi = 40° \cos(\omega t) + 15°$, $d = -1.8cm \sin(\omega t) - 0.4cm$ with variable frequency ω. These verification trajectories are applied to ARASH:ASiST, and to the calibrated LS dynamic model (14), and the corresponding fitness percentage is reported in Table II. As it can be seen from the results reported in this Table, the amount of fitness percentage of the identified model is favorable and remains approximately the same as the fitness percentage of training data. Moreover, by reducing the frequency of the circular trajectory relative to the frequency of the excitation trajectory, the accuracy of the model decreases. It

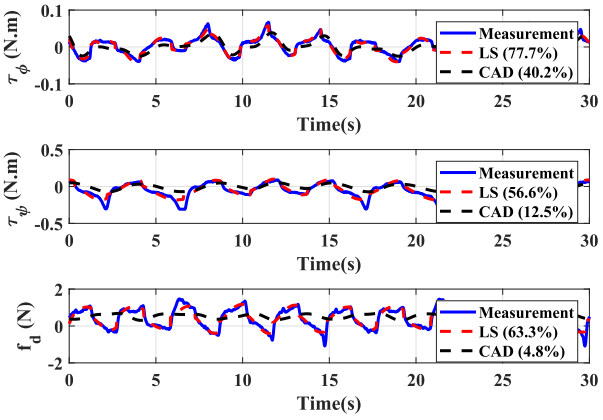

Fig. 4. LS identification of ARASH:ASiST

[2]If a simple controller such as a PD is used, the steady-state error of $\boldsymbol{\tau}$ due to gravitational terms is significant. Thus, such a conclusion cannot be drawn.

[3]Use `filtfilt` command in *MATLAB*.

TABLE I
CALIBRATED BASE INERTIAL PARAMETERS OF ARASH:ASIST WITH LS IDENTIFICATION SCHEME

BIP	Value	$\sigma_{\hat{\pi}_{r_i}}$ %	BIP	Value	$\sigma_{\hat{\pi}_{r_i}}$ %	BIP	Value	$\sigma_{\hat{\pi}_{r_i}}$ %
K_{e3}	+23.7948	0.4231%	π_{r_9}	+0.0726	0.2263%	$\pi_{r_{17}}$	−0.0053	27.4224%
K_{e2}	+0.1431	6.1179%	$\pi_{r_{10}}$	−0.0039	14.9292%	$\pi_{r_{18}}$	−0.0549	19.0854%
F_{c3}	+0.2764	0.3428%	$\pi_{r_{11}}$	+0.0543	2.1096%	$\pi_{r_{19}}$	−0.0030	12.1975%
F_{v3}	+8.6235	0.5510%	$\pi_{r_{12}}$	+0.0082	13.3615%	$\pi_{r_{20}}$	+0.0092	12.3720%
F_{c2}	+0.0302	3.0978%	$\pi_{r_{13}}$	+0.9214	20.0741%	$\pi_{r_{21}}$	+0.0101	22.2809%
F_{v2}	+0.0319	4.5800%	$\pi_{r_{14}}$	−0.9237	20.0291%	$\pi_{r_{22}}$	+0.0020	29.3799%
F_{v1}	+0.0096	8.7376%	$\pi_{r_{15}}$	−0.0016	25.3434%	$\pi_{r_{23}}$	−0.0175	28.1928%
m_7	+0.0056	23.0556%	$\pi_{r_{16}}$	−0.0627	2.0962%			

should be noted that static friction terms have more dominant effect at low speeds, and since training data are based on excitation trajectory, these terms are less excited in the training process.

V. MODEL BASED ROBUST CONTROLLER DESIGN

To verify the use of the obtained calibrated model of the system, while to compensate for other types of uncertainties of the dynamics, the design of a robust controller is considered in this paper. In the proposed robust controller, the controller effort is defined as follows:

$$\begin{aligned}\boldsymbol{\tau} &= \hat{\boldsymbol{M}}(\boldsymbol{q})\ddot{\boldsymbol{q}}_r + \hat{\boldsymbol{C}}(\boldsymbol{q},\dot{\boldsymbol{q}})\dot{\boldsymbol{q}}_r + \hat{\boldsymbol{g}}(\boldsymbol{q}) - \boldsymbol{K}_d\boldsymbol{s} \\ &= \boldsymbol{Y}_{S_r}(\boldsymbol{q},\dot{\boldsymbol{q}},\dot{\boldsymbol{q}}_r,\ddot{\boldsymbol{q}}_r)\hat{\boldsymbol{\pi}}_{r_{(LS)}} - \boldsymbol{K}_d\boldsymbol{s},\end{aligned} \tag{22}$$

in which, the tracking error is denoted by $\boldsymbol{e} = \boldsymbol{q} - \boldsymbol{q}_d$, the desired trajectory is denoted by $\boldsymbol{q}_d$, and $\boldsymbol{q}$ denotes the measured joint space variables. Moreover, virtual reference trajectory $\boldsymbol{q}_r$ is defined as $\boldsymbol{q}_r = \boldsymbol{q}_d - \boldsymbol{\Lambda}\int \boldsymbol{e}dt$, in which $\boldsymbol{s}$ denotes the sliding manifold, and is defined as $\boldsymbol{s} = \dot{\boldsymbol{e}} + \boldsymbol{\Lambda}\boldsymbol{e}$. Furthermore, $\boldsymbol{K}_d$, and $\boldsymbol{\Lambda}$ denote symmetric diagonal positive definite matrices, and $\boldsymbol{Y}_S = [Y_{S_{Links}}, Y_{S_e}, Y_{S_f}]$ denotes reduced Slotine-Li regressor form of the robot, in which, $Y_{S_{Links}}$ may be derived by solution of Ref. [17]. It should be noted that $sign$ functions have been replaced with $tanh/\epsilon$ in friction terms, to avoid *chattering* in real–time control effort.

For motion tracking, the desired trajectory is considered as that detailed in section IV-B with $\omega = 0.5$, and controller gains are set to $\boldsymbol{K}_d = diag(0.4, 0.4, 10)$, and $\boldsymbol{\Lambda} = diag(10, 10, 220)$. The tracking performance of the closed loop system are reported in Figures 5 to 7.

As shown in Figure 6, the surgical instrument has suitably tracked the desired trajectory in the workspace with a maximum error of $128\mu m$ in the insertion direction, and 0.35 deg in rotational motions. This result is very promising for

TABLE II
FITNESS PERCENTAGE OF IDENTIFIED PHYSICAL CONSISTENT LS DYNAMIC MODEL

ω (rad/s)	0.3	0.5	0.7	0.9
$\boldsymbol{\tau}_\phi$	64.42%	68.69%	72.05%	73.84%
$\boldsymbol{\tau}_\psi$	48.76%	50.60%	48.93%	52.59%
$\boldsymbol{f}_d$	49.94%	52.90%	54.55%	56.16%

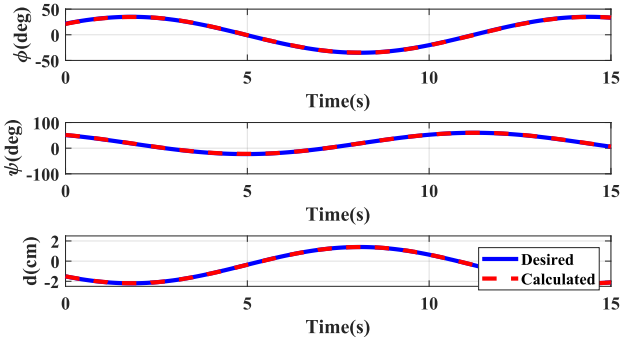

Fig. 5. Motion tracking of ARASH:ASiST, with robust controller

such a simple controller structure. It should be noted that by identifying the robot dynamics parameters and upgrading the model-based controller from previous implemented IDC [4] to the proposed robust controller, the trajectory tracking accuracy has been doubled in all degrees of freedom. To further ensure the accuracy of the applied controller, the desired trajectory with different frequencies $\omega < 0.6$ is reconsidered, and the results show that the maximum tracking error remains at about 0.30° in rotational motions, and $120\mu m$ for linear motion.

VI. CONCLUSIONS, AND FUTURE PROSPECTS

In this paper, the dynamic parameter calibration of ARASH:ASiST, ARAS haptic system for eye surgery training is reported. A linear regression model for the dynamic behavior of the robot is derived, while the dynamic parameters of

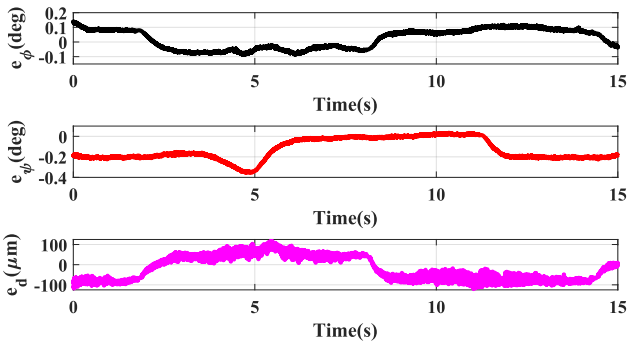

Fig. 6. Motion tracking error of ARASH:ASiST, with robust controller

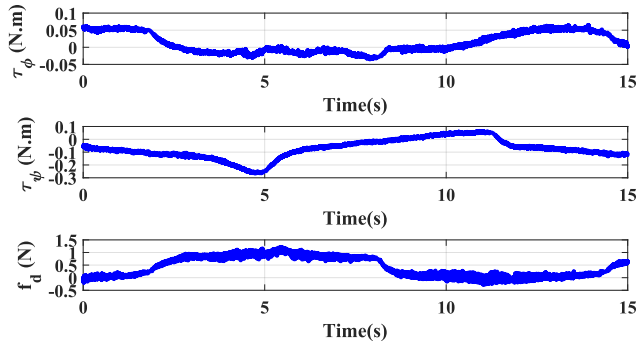

Fig. 7. Control effort of ARASH:ASiST, with robust controller

the robot are calibrated using linear least square (LS) scheme. Cross–validation results for different trajectories indicate that the identified model provides suitable performance. It is shown that the calibrated model developed in this paper is very suitable for different model-based controller design. Implementation of a robust controller results in doubling the tracking performance to some earlier controller structures implemented on the system. It should be noted that like any model, the developed model has still some uncertainties, which may be originated from the following sources.

1) ARASH:ASiST power transmission system is equipped with cable driven mechanism. Since steel cables properties change over time due to cable stretch and creep, there is always deformation in the cables that cause: $\boldsymbol{q}_{Motor} \neq \boldsymbol{q}_{Joint}$. In rotational motion ϕ, fortunately, the cable length in the proposed design is not long, and the effect of cable deformation becomes negligible. However, in ψ and d, this issue remains as a source of uncertainty in the model, and to overcome this issue the solution proposed in [18] which is developed for the *Raven-II surgical robot* could be used in our design as well.
2) As shown in Figure 1, some electrical wiring are connected to the end-effector, which plays as a variable disturbance to the system, and influence on the accurate weight compensation of the robot. This will introduce a steady error in ψ. This issue is also experienced in [19], for *Da Vinci surgical robot* and a high-order polynomial model of this variable disturbance is proposed to be used.
3) In some applications, for example, IDC with identified dynamic parameters, it is important to ensure that the identified parameters $\boldsymbol{\pi}$ have are becoming positive definite, e.g. $\boldsymbol{M}$. Convex optimization-based solution of Ref. [8], which was developed for *Da Vinci surgical robot*, may be considered as a proper method to consider physical consistency constraints in LS identification.

ACKNOWLEDGMENT

This work is supported in part by the National Institute for Medical Research Development (NIMAD) under Grant No. 4001546, and Iran National Science Foundation (INSF) Synergy Grant No. 99021926.

REFERENCES

1 M. Motaharifar, A. Norouzzadeh, P. Abdi, A. Iranfar, F. Lotfi, B. Moshiri, A. Lashay, S. F. Mohammadi, and H. D. Taghirad, "Applications of haptic technology, virtual reality, and artificial intelligence in medical training during the covid-19 pandemic," *Frontiers in Robotics and AI*, p. 258, 2021.
2 M. J. Gerber, M. Pettenkofer, and J.-P. Hubschman, "Advanced robotic surgical systems in ophthalmology," *Eye*, vol. 34, no. 9, pp. 1554–1562, 2020.
3 M. Motaharifar, H. D. Taghirad, K. Hashtrudi-Zaad, and S. F. Mohammadi, "Control synthesis and iss stability analysis of a dual-user haptic training system based on s-shaped function," *IEEE/ASME Transactions on Mechatronics*, vol. 24, no. 4, pp. 1553–1564, 2019.
4 A. Hassani, M. Dindarloo, R. Khorambakht, A. Bataleblu, H. Sadeghi, R. Heidari, A. Iranfar, P. Hasani, N. Hojati, A. Khorasani, N. KhajeAhmadi, M. Motaharifar, H. Riazi-Esfahani, A. Lashay, S. F. Mohammadi, and H. D. Taghirad, "Kinematic and dynamic analysis of arash asist: Toward micro positioning," in *2021 9th RSI International Conference on Robotics and Mechatronics (ICRoM)*. IEEE, nov 2021, pp. 59–65.
5 G. A. Fontanelli, F. Ficuciello, L. Villani, and B. Siciliano, "Modelling and identification of the da vinci research kit robotic arms," in *2017 IEEE/RSJ International Conference on Intelligent Robots and Systems (IROS)*. IEEE, 2017, pp. 1464–1469.
6 J. Wu, J. Wang, and Z. You, "An overview of dynamic parameter identification of robots," *Robotics and computer-integrated manufacturing*, vol. 26, no. 5, pp. 414–419, 2010.
7 M. Gautier, "Numerical calculation of the base inertial parameters of robots," *Journal of robotic systems*, vol. 8, no. 4, pp. 485–506, 1991.
8 Y. Wang, R. Gondokaryono, A. Munawar, and G. S. Fischer, "A convex optimization-based dynamic model identification package for the da vinci research kit," *IEEE Robotics and Automation Letters*, vol. 4, no. 4, pp. 3657–3664, oct 2019.
9 A. Bataleblu, R. Khorrambakht, and H. D. Taghirad, "Robust H∞-based control of ARAS-diamond: A vitrectomy eye surgery robot," *Proceedings of the Institution of Mechanical Engineers, Part C: Journal of Mechanical Engineering Science*, p. 095440622097933, dec 2020.
10 H. D. Taghirad, *Parallel robots: mechanics and control*. CRC press, 2013.
11 D. Jung, J. Cheong, D. I. Park, and C. Park, "Backward sequential approach for dynamic parameter identification of robot manipulators," *International Journal of Advanced Robotic Systems*, vol. 15, no. 1, p. 1729881418758578, 2018.
12 J. Klodmann, D. Lakatos, C. Ott, and A. Albu-Schäffer, "A closed-form approach to determine the base inertial parameters of complex structured robotic systems," *IFAC-PapersOnLine*, vol. 48, no. 1, pp. 316 – 321, 2015, 8th Vienna International Conferenceon Mathematical Modelling.
13 E. Dombre and W. Khalil, Eds., *Modeling, Performance Analysis and Control of Robot Manipulators*. ISTE, jan 2007.
14 H. D. Taghirad and P. R. Belanger, "Modeling and Parameter Identification of Harmonic Drive Systems," *Journal of Dynamic Systems, Measurement, and Control*, vol. 120, no. 4, pp. 439–444, 12 1998.
15 J. Swevers, C. Ganseman, D. Tukel, J. de Schutter, and H. V. Brussel, "Optimal robot excitation and identification," *IEEE Transactions on Robotics and Automation*, vol. 13, no. 5, pp. 730–740, 1997.
16 L. Ljung and R. Singh, "Version 8 of the matlab system identification toolbox," *IFAC Proceedings Volumes*, vol. 45, no. 16, pp. 1826–1831, 2012.
17 J. Yuan and B. Yuan, "Recursive computation of the slotine-li regressor," in *Proceedings of 1995 American Control Conference-ACC'95*, vol. 3. IEEE, 1995, pp. 2327–2331.
18 M. Haghighipanah, Y. Li, M. Miyasaka, and B. Hannaford, "Improving position precision of a servo-controlled elastic cable driven surgical robot using unscented kalman filter," in *2015 IEEE/RSJ international conference on intelligent robots and systems (IROS)*. IEEE, 2015, pp. 2030–2036.
19 H. Lin, C.-W. V. Hui, Y. Wang, A. Deguet, P. Kazanzides, and K. S. Au, "A reliable gravity compensation control strategy for dvrk robotic arms with nonlinear disturbance forces," *IEEE Robotics and Automation Letters*, vol. 4, no. 4, pp. 3892–3899, 2019.